

Three-Dimensional Atom Probe Investigation of Microstructural Evolution during Tempering of an Ultra-High-Strength High-Toughness Steel

R. VEERABABU, R. BALAMURALIKRISHNAN, K. MURALEEDHARAN, and M. SRINIVAS

The evaluation of the tempering response of an ultra-high-strength, high-toughness (UHSHT) steel revealed that samples austenitized at 900 °C and tempered for 4 and 8 hours at 485 °C had similar yield strengths but a ~50 pct increase in fracture toughness for the 8-hour temper. The results of our investigations of microstructural origins of this difference, using the nanometric scale resolution of the three-dimensional atom probe (3DAP) suggest that nanoscale strengthening precipitates, essentially carbides and intermetallic clusters (containing primarily Cr and Mo atoms), are present in both samples. The chemical compositions of the particles in the two samples were found to be similar, but clear evidence of differences in physical attributes of the precipitates, such as particle size, morphology, and interparticle spacing, are seen.

DOI: 10.1007/s11661-007-9333-0

© The Minerals, Metals & Materials Society and ASM International 2007

I. INTRODUCTION

THE three-dimensional atom probe (3DAP) is a unique tool capable of yielding chemical information at the atomic level, and, in conjunction with the well-known techniques of transmission electron microscopy (TEM), offers a powerful way of studying the microstructure of materials at the submicron scale. In recent years, the 3DAP is being used to investigate microstructural phenomena occurring at nanometric scale, approaching near atomic dimensions.^[1–7] These studies have proved invaluable in developing a better understanding of structure-property correlations, especially the influence of nanometric scale microstructural features on mechanical behavior. Further, the studies have helped elucidate fundamental issues pertaining to thermodynamic and kinetic aspects of microstructural evolution. One important area of scientific and industrial importance, where the capabilities of the 3DAP can be invaluable, is in the investigation of ultra-high-strength high-toughness (UHSHT) steels. This article describes how we have used a 3DAP to investigate the microstructural evolution in a UHSHT steel that is being developed in our laboratory, and to understand the structure-property correlations.

UHSHT steels, in the properly heat-treated condition, exhibit an unparalleled combination of strength and

fracture toughness and hence find use in niche applications such as aircraft landing gear components. Typical compositions and mechanical properties of some representative UHSHT steels are given in Tables I and II, respectively. Extensive research^[8–11] has gone into the development of HY180, AF1410, and Aermet 100 steels to achieve the best combination of strength and fracture toughness, in addition to excellent stress corrosion cracking resistance, through a tailoring of the microstructure by optimizing composition and heat treatment. In all these steels, the target microstructure primarily consists of a recovery-resistant heavily dislocated martensitic matrix^[13] and the precipitates that are responsible for secondary hardening. The desired microstructure is achieved by additions of Ni and Co (to obtain the matrix properties) and of Cr and Mo (for obtaining the secondary hardening precipitates, essentially M_2C carbides). It can be seen (Table I) that while HY180, an early variant, contains 8 wt pct Co and 10 wt pct Ni, the other steels contain both Co and Ni in excess of 10 pct. The levels of Cr and Mo, around 2 and 1 wt pct, respectively, in both HY180 and AF1410, have been increased slightly in the Aermet grades. The extent of carbon has also progressively increased, from 0.10 wt pct in HY180 to ~0.25 wt pct in Aermet 100 and Aermet 310, mainly to achieve higher base strength levels. Extensive microstructural investigations, particularly on AF1410,^[8,13] have shown that inter- and intra-lath alloy cementite (M_3C , $M = Fe, Cr, Mo$) particles are present in the microstructure in addition to the M_2C carbides. Iorio *et al.*^[8] have shown that, in AF1410, significant amounts of cementite are present even in the optimized heat-treatment condition (*i.e.*, after tempering for 5 hours at 510 °C), and that the extent of cementite precipitation is much more strongly influenced by the carbon level of the steel than by the concentrations of Cr and Mo. The presence of cementite in these steels is

R. VEERABABU, R. BALAMURALIKRISHNAN, K. MURALEEDHARAN, and M. SRINIVAS, Scientists, are with the Defence Metallurgical Research Laboratory, Kanchanbagh, Hyderabad 500 058, India. Contact e-mail: muraleek@hotmail.com

This article is based on a presentation given in the symposium entitled "Materials Behavior: Far from Equilibrium" as part of the Golden Jubilee Celebration of Bhabha Atomic Research Centre, which occurred December 15–16, 2006 in Mumbai, India.

Article published online October 27, 2007

Table I. Composition (Weight Percent) of Typical Secondary Hardening Steels

Steel	C	Co	Ni	Cr	Mo	V	Fe
HY180 ^[8]	0.10	8.0	10.0	2.0	1.0	—	bal
AF1410 ^[8]	0.16	14.0	10.0	2.0	1.0	—	bal
Aermet100 ^[9]	0.24	13.4	11.5	3.0	1.2	—	bal
Aermet 310 ^[9]	0.25	15.0	11.0	2.4	1.4	—	bal

generally believed to be detrimental to both strength and toughness. Therefore, it is desirable to explore whether the secondary hardening effect can be enhanced by minimizing the amount of cementite, perhaps by a uniform and finer dispersion of other precipitates, such as M₂C- or MC-type carbides. All the steels listed in Table I are typically used in the peak toughness condition, which corresponds to a slightly overaged microstructure, with respect to strength and hardness.

In these steels, the carbon level is below about 0.25 wt pct. We have an ongoing program^[12] in our laboratory to develop an UHSHT steel with ~0.35 wt pct carbon (Table III) to achieve YS > 1700 MPa, UTS > 2000 MPa, and $K_{IC} \sim 100$ MPa√m. We have also added about 0.2 wt pct V primarily as a grain refiner, but also to explore whether the formation of MC-type carbides during tempering may be used to minimize the extent of alloy cementite. In this experimental alloy, the Cr and Mo content have been retained at levels similar to those used in HY180 and AF1410. During the investigation of the mechanical properties of this alloy under different heat-treatment conditions, it was found that two samples, austenitized at a temperature of 900 °C and tempered at 485 °C for 4 and 8 hours, respectively, had similar strength levels, but the latter exhibited a fracture toughness nearly 50 pct greater than that of the former (Table IV). The purpose of the work reported in this article is to highlight the utility of the 3DAP in addressing the microstructural origins of the difference in fracture toughness between the two samples.

II. EXPERIMENTAL METHODOLOGY

The details of the alloy development program, including the melting, plate rolling, heat treatment, and tempering response and mechanical properties of the experimental alloy under different heat-treatment conditions, will be published elsewhere. Briefly, the material

Table III. Composition (Weight Percent and Atomic Percent) for DMRL Experimental Steel

	C	Co	Ni	Cr	Mo	V	Fe
Wt pct	0.37	14.80	13.70	2.00	1.00	0.20	67.93
At. pct	1.73	14.07	13.08	2.16	0.58	0.22	68.16

was produced in a 40-kg batch by vacuum induction melting of electrolytically pure raw materials and pouring, under vacuum, into a rectangular mold of 100 × 300 mm cross section. The resultant ingot was homogenized at 1050 °C for 24 hours and subsequently radiographed, and the defective “pipe” portions were removed. The sound portion of the ingot was soaked at 1050 °C for 4 hours and hot rolled into 15-mm-thick plates. Samples from the plates were austenitized at either 900 °C, 950 °C, or 1000 °C, and then subjected to tempering at different temperatures ranging from 455 °C to 510 °C for times varying from 15 minutes to 24 hours. The tempering response as a function of tempering time for each combination of austenitizing and tempering temperatures was followed using Vicker’s hardness measurements, using 30-kgf load. Room-temperature tensile properties and fracture toughness were determined, on samples machined from the heat-treated blanks, following the standard ASTM testing procedures.

Samples for scanning electron microscopy (SEM) studies were cut from the tempered blanks, mounted, mechanically polished using standard metallographic procedures, and lightly etched with 2 pct nital. Thin foils for TEM examination were prepared from material obtained from the grip region of the tensile tested samples: ~200-μm thick slices were cut using a slow speed saw, mechanically ground to ~100-μm thickness, and subsequently twin jet electropolished with mixed acids (by volume: 78 pct methanol, 10 pct lactic acid, 7 pct sulfuric acid, 3 pct nitric acid, and 2 pct hydrofluoric acid) electrolyte at -30 °C. The thin foils were examined in a FEI Tecnai 20T transmission electron microscope operated at 200 kV and equipped with an EDAX EDS system.

The atom probe specimens were prepared by a standard two-stage electropolishing procedure, as described by Miller and Smith.^[15] Initially, 15 to 20 mm long blanks with 0.3- to 0.5-mm-diameter were cut from tensile-tested samples using wire EDM. In the first stage, a solution of 25 pct perchloric acid in glacial acetic acid

Table II. Representative Mechanical Properties of Secondary Hardening Steels in Table I

Steel	Heat Treatment		Yield Strength (MPa)	Tensile Strength (MPa)	Fracture Toughness (K_{IC} , MPa√m)
	Austenitizing Temperature (°C)/Time (h)	Tempering Temperature (°C)/Time (h)			
HY180 ^[10]	899/1 h + 825/1 h	510/5 h	1250	1380	233
AF1410 ^[10]	899/1 h + 825/1 h	510/5 h	1533	1675	158
Aermet 100 ^[9]	899/1 h + 825/1 h	510/5 h	1724	1965	126
Aermet 310 ^[9]	912/1 h	482/5 h	1896	2172	71

Table IV. Mechanical Properties of Two Samples of DMRL Experimental Steel

Heat Treatment		Yield Strength* (MPa)	Tensile Strength* (MPa)	Fracture Toughness** (K_{IC} , MPa \sqrt{m})
Austenitizing Temperature (°C)/Time (h)	Tempering Temperature (°C)/Time (h)			
900/1 h	485/4 h	1855	2105	45
900/1 h	485/8 h	1825	2040	66

*From tensile tests^[12] performed according to ASTM E-8.

**Estimated from J_Q tests^[12] per ASTM E-813 and, after checking validity, converted to K_{IC} using $J_{IC} = \sqrt{K_{IC} E (1-\nu^2)}$, where E = Young's modulus and ν = Poisson's ratio.

was used at 5 to 15V DC to thin the shank diameter of the blanks and to obtain a rough conical shaped tip. In the second stage, the final tip was formed by pulse micropolishing, initially using a solution of 6 pct perchloric acid in glacial acetic acid, and subsequently using 2 pct perchloric acid in 2-butoxy ethanol at 5 to 20 V DC.

Atom probe experiments were carried out employing a 3DAP with a field ion microscope (FIM) instrument manufactured by Oxford NanoScience Ltd., Milton Keynes, United Kingdom (presently a subsidiary of Imago, Madison, WI). Field ion images were recorded at a specimen temperature of 70 K with neon as the imaging gas at $\sim 2.5 \times 10^{-5}$ mbar pressure. Once a clean field ion image was obtained, the region of interest was chosen and positioned for atom probe data acquisition, which was performed at pressures below 8×10^{-10} mbar using a 15 pct pulse fraction. Data reconstruction, analysis, and visualization were performed using the PoSAP software supplied with the instrument. The presence of solute-enriched precipitates/clusters and their compositions was determined with the maximum separation envelope method,^[16] which was successfully employed by several researchers.^[17–26] This was done using a built-in module in PoSAP with the following parameters: minimum number of atoms in the particle, $N_{\min} = 10$; maximum (solute) separation distance, $d_{\max} = 0.4$ nm; surrounding distance = 0.2 nm; and erosion distance = 0.2 nm. A detection efficiency of 0.5 has been assumed.

III. RESULTS AND DISCUSSION

A. Scanning Electron Microscopy and Transmission Electron Microscopy

Because the austenitizing and tempering temperatures for both 4- and 8-hour tempered samples are identical, microstructural features such as prior austenite grain size, martensitic lath colony size, lath width, amount of retained austenite, and particles retained from austenitizing temperature are expected to be similar. This implies that major differences in microstructure between the two samples are likely to be those that evolve during tempering, especially the hardening precipitates.

The SEM images reveal the expected lath martensitic structure (Figure 1), with no noticeable differences between the two samples. Bright- and dark-field TEM micrographs (Figure 2) show the presence of several particles and a heavily dislocated lath martensitic matrix. Detailed analyses of several dark-field micrographs of both samples revealed the presence of a bimodal size distribution for the particles. The coarser particles have sizes ranging from 20 to 80 nm and are found predominantly at lath boundaries; however, a few were seen both at prior austenite grain boundaries and occasionally in the interior of the laths. It is reasonable to suppose that the interlath particles have arisen from the decomposition of interlath austenite films during tempering, while those seen at prior austenite grain boundaries and lath interiors are retained from the austenitizing temperature of 900 °C. Our work^[12] has shown that austenitizing temperatures greater than

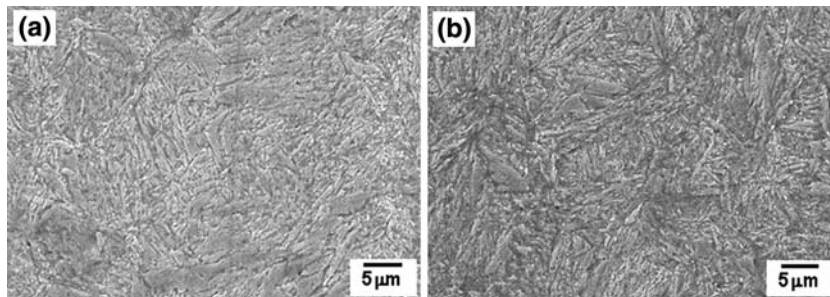


Fig. 1—Scanning electron micrographs showing the lath microstructure for the samples austenitized at 900 °C and tempered at 485 °C for (a) 4 h and (b) 8 h.

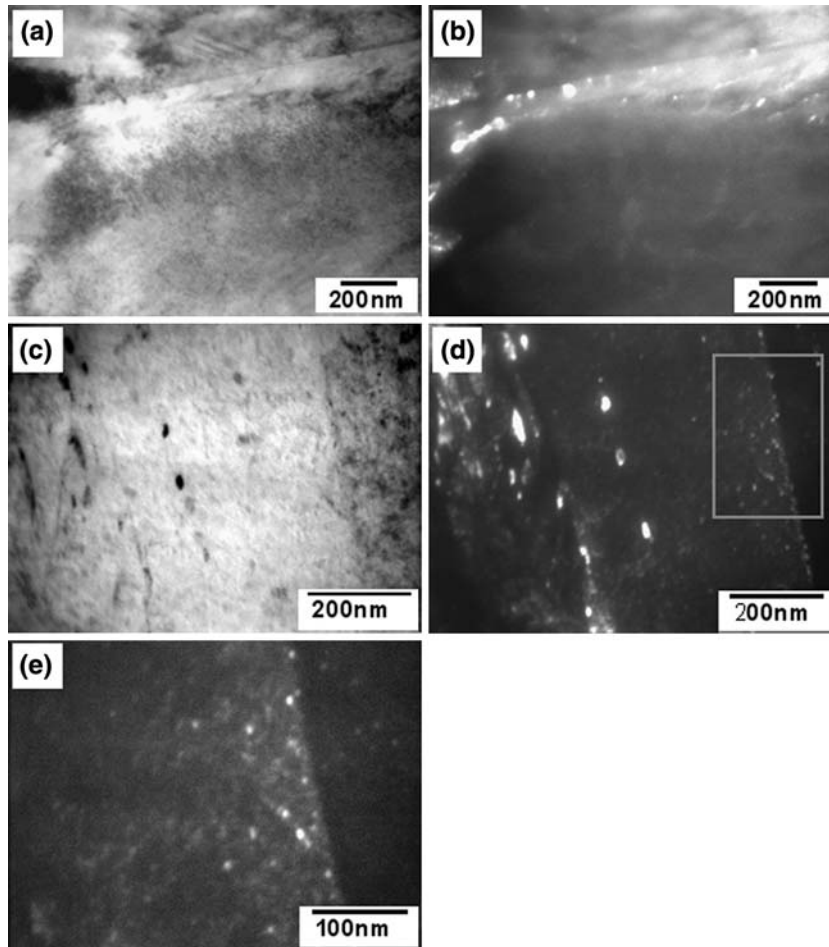


Fig. 2—TEM micrographs: (a) and (b) bright-field, dark-field pair for the 4-h tempered sample; (c) and (d) bright-field, dark-field pair for the 8-h tempered sample; and (e) high-magnification picture of the region indicated in (d) showing the fine particles.

950 °C are required to dissolve these particles. This is similar to the observations reported by Raghavan Ayer and Machmeier^[27] on Aermet 100 steel. The interlath coarse particles are found to possess high aspect ratio morphology, being elongated along the direction of the lath boundary. The energy dispersive spectra (Figure 3) obtained from the coarse particles, both interlath and

those found at austenite grain boundary/lath interiors, showed them to be, relative to the matrix, enriched in Cr, Mo, and C, with varying (particle-to-particle) relative enrichments of Mo and Cr. In spite of their relatively larger size, the presence of definite interference from the matrix precludes a more quantitative analysis of the chemical composition of these particles.*

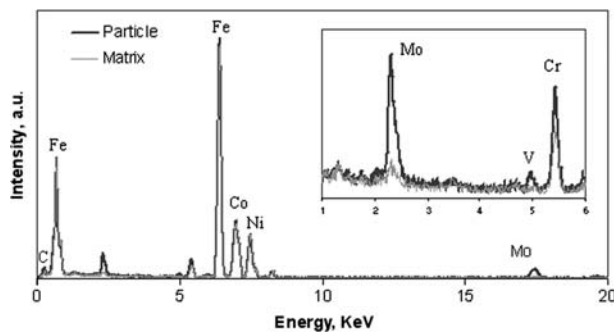


Fig. 3—EDS spectra from one of the coarse particles and the matrix in the sample tempered for 4 h. Inset shows the strong enrichment of Mo, and a weak enrichment of Cr and V in the particle relative to the matrix.

*More quantitative analysis on the coarser particles might be possible by the use of extraction replicas, but that is beyond the scope of the present work, which focuses on features amenable to investigation by atom probe.

In contrast, the finer particles had sizes below about 10 nm, with an average size of ~5 nm, and were found both at lath boundaries and in the interior of laths (Figures 2(d) and (e)). The spatial distribution of the finer particles appears to be fairly uniform throughout the material.

This bimodal size distribution is similar to the results reported by Allen *et al.*^[13] in AF1410 steel that had been solutionized at 830 °C and subsequently aged at 510 °C for 10 hours. In that work based on SANS and TEM, the authors have attributed the finer size distribution to

M₂C-type carbides and the coarser size distribution to M₃C-type particles. As mentioned earlier, Iorio *et al.*^[8] have also reported the presence of inter- and intra-lath alloy cementite particles, having similar sizes, in AF1410 as well as Aermet 100 after different tempering cycles. Based on our work^[12] and literature reports, we expect the larger particles in our experimental steel to be M₃C type and the finer ones to be M₂C type. The latter form the focus of the work reported here.

B. Field Ion Microscopy

The FIM images obtained with neon as imaging gas at 70 K at different specimen voltages are given in Figure 4. At a specimen voltage of 8.5 kV (Figure 4(a)), individual dots as well as brightly imaging clusters can be seen; the former are attributed to the matrix, whereas the latter are due to the precipitates/clusters. As the specimen voltage is increased (Figures 4(b) and (c)), the contrast between the matrix and the precipitates/clusters is increased, until, at a specimen voltage of 13 kV, only the precipitates/clusters are seen and the atoms in the matrix regions are not at all imaged (Figure 4(d)). While it is nontrivial to estimate the sizes, it can be seen that the precipitates have a wide size- and shape-distribution.

C. 3DAP Characterization

The individual atom positions for the different elements in the 4-hour tempered sample are shown in Figure 5. It can be seen that carbon, chromium, and molybdenum are not uniformly distributed, with evidence of precipitate/cluster formation. However, vanadium, in spite of being a strong carbide former, does not exhibit the same behavior. We have quantified the deviation from randomness of the spatial distributions

of all the elements by comparison with appropriate binomial distributions.^[28] From this, we have confirmed that, indeed, vanadium shows only a weak departure from a random distribution and also that the distribution of Ni and Co atoms is fairly random.

1. Particle/cluster analyses

Figure 6 shows a comparison of the spatial distribution of the solute elements, in a selected subvolume, in the 4- and the 8-hour tempered samples. The partitioning of C, Cr, and Mo to the precipitates/clusters is stronger in the 8-hour sample relative to the 4-hour sample. In order to identify and analyze the particles/clusters, carbon and the three carbide forming elements (Cr, Mo, and V) were chosen as the solute elements. The maximum separation envelope method, with parameters as given in Section II, detected the presence of 111 and 98 particles in the 4- and 8-hour tempered samples, respectively, which correspond to a number density of 2.13×10^{25} and $1.62 \times 10^{25}/\text{m}^3$ in the two cases. Thus, the number density has decreased by nearly 25 pct in the 8-hour tempered sample relative to the 4-hour tempered sample.

Figure 7 shows the same representative subvolumes, as shown in Figure 6, but only atoms identified as belonging to particles/clusters have been rendered. It can be seen that the particles in the 8-hour sample (Figure 7(b)) are, on average, coarser than those in the 4-hour sample (Figure 7(a)). In these figures, iron atoms have also been rendered in addition to the solute atoms for two purposes: first, to confirm the efficiency of the “erosion” process in the particle detection algorithm to ensure that matrix iron atoms are not counted as part of the particle, and second to show that there are indeed iron atoms inside the particle, which must be counted as belonging to the particle and therefore considered for

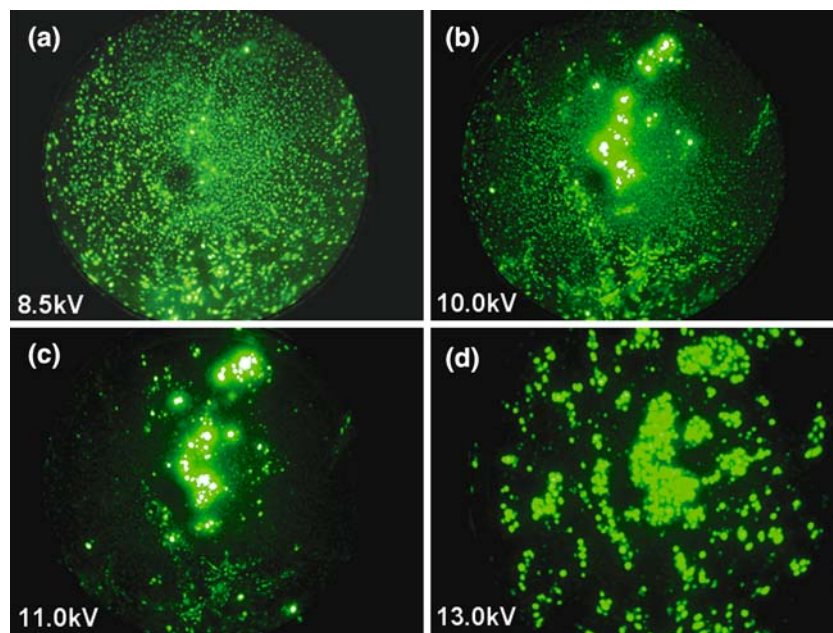


Fig. 4—FIM images of a typical UHSHT steel sample in the quenched and tempered condition at different sample voltages.

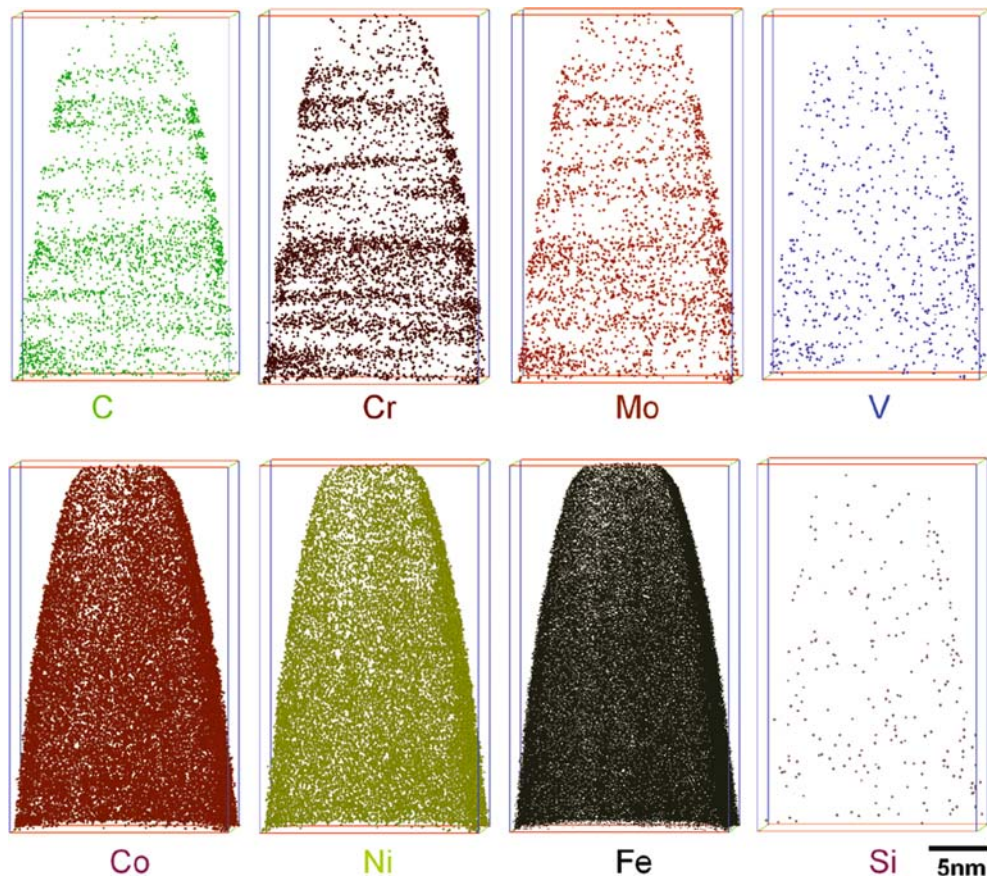


Fig. 5—Atom maps for various elements in the 4-h tempered sample.

any quantification/chemical composition analysis. While Ni and Co atoms have been included in the composition analysis of particles, they have not been rendered for the sake of clarity.

We have determined the sizes of the particles/clusters using two methods, one based on the Guinier radius^[28] and another based on the number of atoms, n , detected in the particle.^[28]

$$R = (3n\Omega/4\pi\zeta)^{1/3}$$

where Ω , the atomic volume, is $1.178 \times 10^{-2} \text{ nm}^3$ for bcc Fe, and ζ , the overall detection and reconstruction efficiency, has been taken to be 0.5. Comparison with recent simulations by Miller and Russell^[29] shows that both these methods are likely to underestimate the actual sizes of the clusters/precipitates. It is expected that the latter method, based on the number of ions, is a better indicator of the true feature size in the present case. Nevertheless, either method can be used to study overall trends in the average size and the size distributions.

Based on the Guinier radius, the average size of the particles/clusters was determined to be $0.37 \pm 0.02 \text{ nm}$ and $0.44 \pm 0.05 \text{ nm}$ for the 4- and 8-hour tempered samples, respectively, while the one based on the number of ions yielded average sizes of $0.55 \pm 0.03 \text{ nm}$ and $0.61 \pm 0.06 \text{ nm}$ for the two samples, respectively (Table V). The percentage frequency size distributions for the two samples are given in Figure 8. It can be seen that a

majority of the particles, in both samples, have sizes in the 0.4- to 1.0-nm range. Attempts to detect crystallographic planes were largely unsuccessful, suggesting that these might be “clusters” or embryonic precursors to the formation of crystalline particles, which have been seen as the finer particles in the TEM dark-field images that have been formed using specific, but unindexed, diffraction spots. The smallest of these crystalline particles (~ 2 to 4 nm in size) may not be readily seen in TEM, particularly in view of the heavily dislocated martensitic matrix in which they are present. Conversely, in view of the sampling volume limitations in the atom probe, the chances of encountering larger particles is much smaller—only one particle with a radius $> 1.3 \text{ nm}$ was seen in the 4-hour tempered sample, and two particles, with radii larger than 1.9 and 2.4 nm, respectively, were seen in the 8-hour tempered sample. The exact size of these particles could not be estimated as they extended beyond the analysis volume. Analysis of many more samples may be required before any conclusions can be drawn regarding these particles.

2. Chemical composition

The chemical composition of the clusters was first analyzed in terms of the carbon concentration due to the fact that the fine precipitates expected to be present are coherent M_2C carbides. Stoichiometric M_2C contains 33 at. pct C. However, it is known that M_2C is often

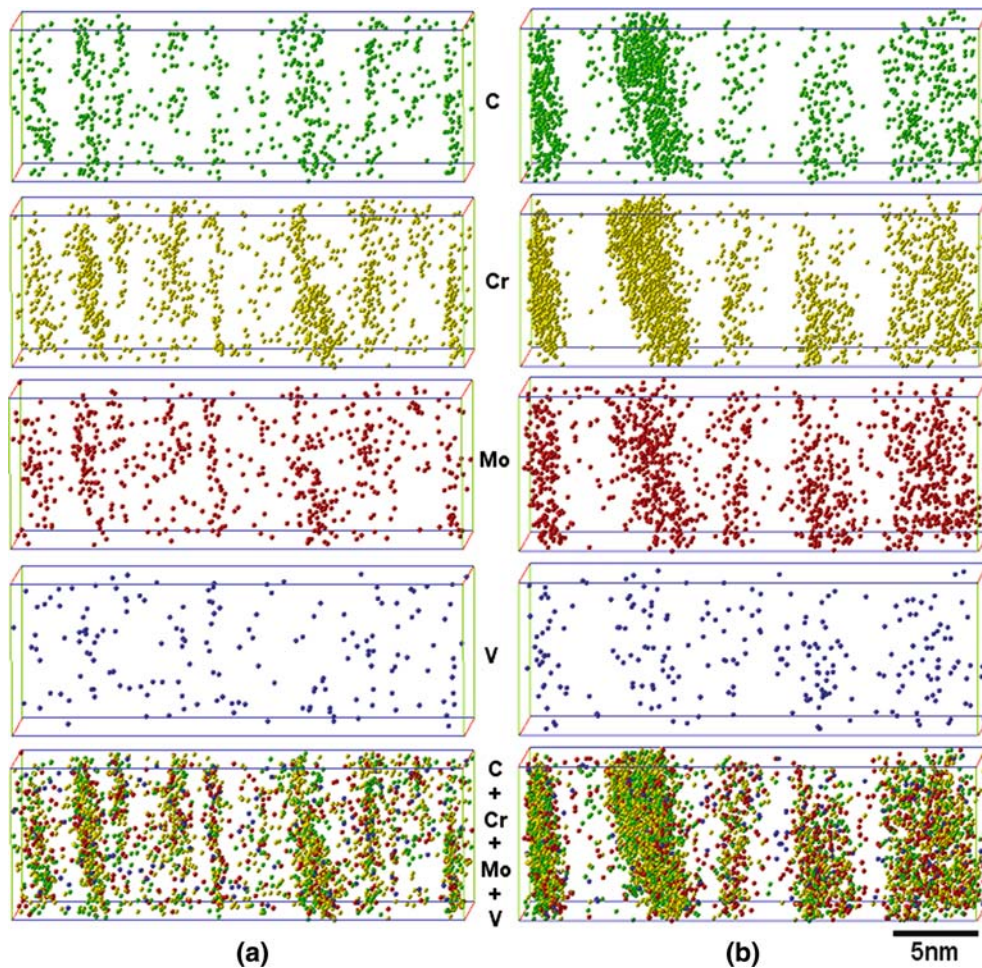


Fig. 6—3D reconstructed atom maps from selected subvolumes for the samples tempered at (a) 4 h and (b) 8 h.

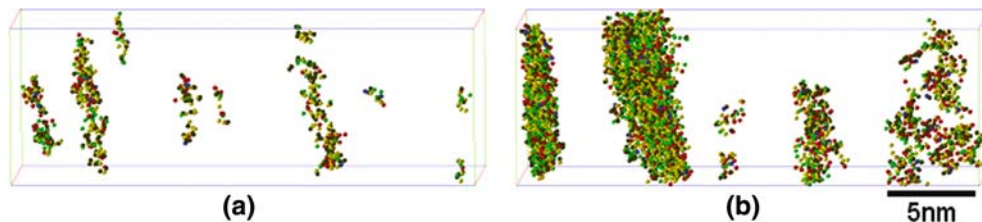


Fig. 7—3D reconstructed atom maps for (a) 4-h and (b) 8-h tempered samples showing only atoms identified as being present in the precipitates/clusters. The color code is the same as for Fig. 6. Only solute atoms and iron atoms (dark green) are shown.

Table V. Average Size of the Clusters in 4- and 8-Hour Tempered Samples

Size Parameter	4 h	8 h
Guinier radius, ^[28] nm	0.37 ± 0.02	0.44 ± 0.05
Radius based on number of ions, ^[28] nm	0.55 ± 0.03	0.61 ± 0.06

carbon deficient. It has been reported^[13,30,31] that, in AF1410 steel tempered at 510 °C, the carbon content is only ~14 at. pct (corresponds to $M_2C_{0.32}$) after 1 hour of tempering, and about 23 at. pct ($M_2C_{0.6}$) up to 4 hours

of tempering; the carbon content increases to about 29 pct ($M_2C_{0.8}$) only after 10 hours of tempering, and full stoichiometry is achieved only for tempering times longer than 24 hours. Thus, it may be argued that all M_2C -type particles are carbon deficient in the early stages and the carbon content progressively increases with tempering time.

The percentage frequency distribution histograms as a function of carbon content for the 4- and 8-hour tempered samples are shown in Figure 9. It is clear that, in both cases, the clusters possess varying levels of carbon, ranging from 0 to 40 at. pct. Based on the discussion in the preceding paragraph, we might

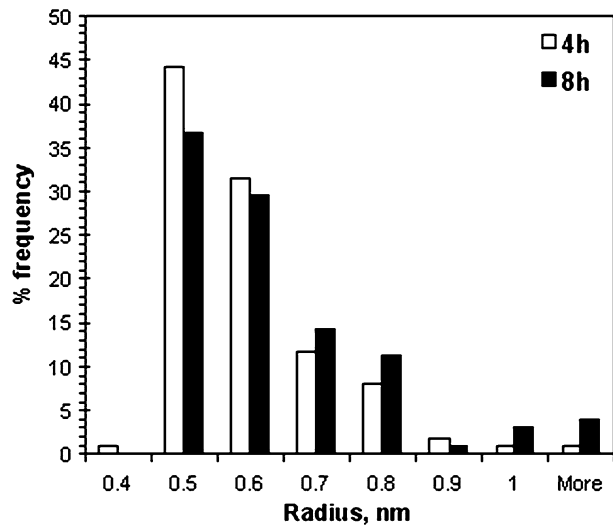


Fig. 8—Size distribution of the clusters in samples tempered for 4 h and 8 h. Sizes based on the number of ions in the cluster have been used.

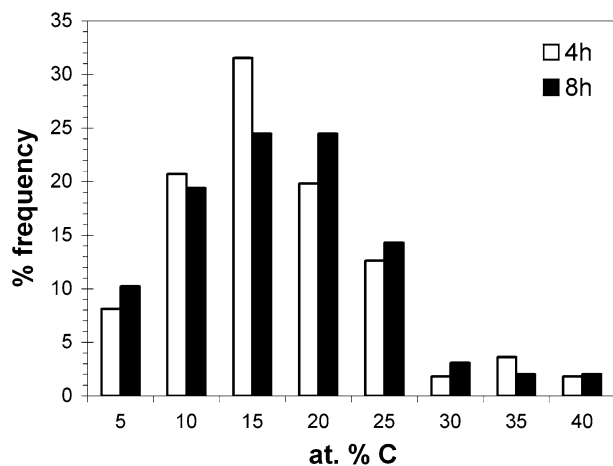


Fig. 9—Percentage frequency histograms as a function of carbon concentration in the clusters for 4- and 8-hour tempered samples.

consider clusters with more than 10 at. pct carbon to be carbide precursors and those with lesser carbon concentration to be intermetallic co-clusters. While this demarcation is somewhat arbitrary, it does confirm that several carbon-deficient (intermetallic) clusters are present in both the samples, comprising nearly 30 pct of the clusters observed in either sample. The average sizes of the intermetallic and the carbon containing clusters are similar for a given tempering condition (Table VI), but, interestingly, in either sample, clusters containing more than 100 ions have carbon content in excess of 10 at. pct. This indicates that larger intermetallic clusters ($n > 100$ ions) are perhaps not stable in this material for the tempering conditions investigated. However, the presence of the finer intermetallic clusters is proved beyond doubt. These clusters might play an important role in influencing the mechanical properties such as strength and fracture toughness of the material.

Table VI. Comparison of Average Size of Carbon-Deficient (Intermetallic) and Carbon-Rich Clusters in 4- and 8-Hour Tempered Samples

Cluster Type	Average Size, nm	
	4 h	8 h
Carbon-deficient (intermetallic), C < 10 at. pct	0.53 ± 0.08	0.56 ± 0.09
Carbon-rich (C \geq 10 at. pct)	0.55 ± 0.12	0.59 ± 0.17

Stack plots illustrating the composition of the clusters in the two samples are given in Figure 10. The data have been plotted in terms of increasing carbon content (left to right). The concentration of Cr, Mo, and Fe show a wide variation, ranging from 5 to 50 pct. This large variation is perhaps due to the small size of the clusters (which means that there are more atoms on the surface than in the interior) and the inherent nature of the particle detection algorithm. Detailed analysis has revealed that no simple correlation exists between the size and composition in either the 4- or 8-hour tempered condition for clusters with radius less than 0.825 nm (corresponds to 100 detected atoms).

The average chemical composition of the carbon-rich and carbon-deficient clusters is given in Table VII. The high values of standard deviation quantify the large scatter in composition; nevertheless, trends in compositional changes may be inferred with reasonable accuracy. In the 4-hour tempered sample, Mo and Fe are significantly enriched in intermetallic clusters relative to carbon-rich clusters. A similar trend is seen in the 8-hour tempered sample. Also, the average Mo content in either type of cluster increases with the increase in tempering time, while the average Cr content decreases.

Larger clusters ($r > 0.825$ nm), all of which are carbon-rich, differ much less in their composition—the clusters have an average composition (in atomic percent) of 26Fe-31Cr-13Mo-3V-17C in the 4-hour tempered sample and 25Fe-31Cr-16Mo-3V-19C in the 8-hour tempered sample. Except for a marginal enrichment of carbon and molybdenum in the 8-hour sample, the compositions are similar in the two conditions.

IV. SUMMARY AND CONCLUSIONS

The atom probe has been shown to be useful in accessing microstructural information at the nanometric scale normally not available by other techniques. We have investigated, using the 3DAP, two samples of an experimental UHSHT steel that have been austenitized at 900 °C and tempered at 485 °C for 4 and 8 hours, respectively, in order to explore the microstructural origins of a nearly 50 pct increase in toughness, without loss of strength, for the 8-hour tempered sample relative to the 4-hour tempered sample. The main observations are as follows.

1. A 25 pct decrease in the number density and an 11 pct increase in the size of the clusters in the

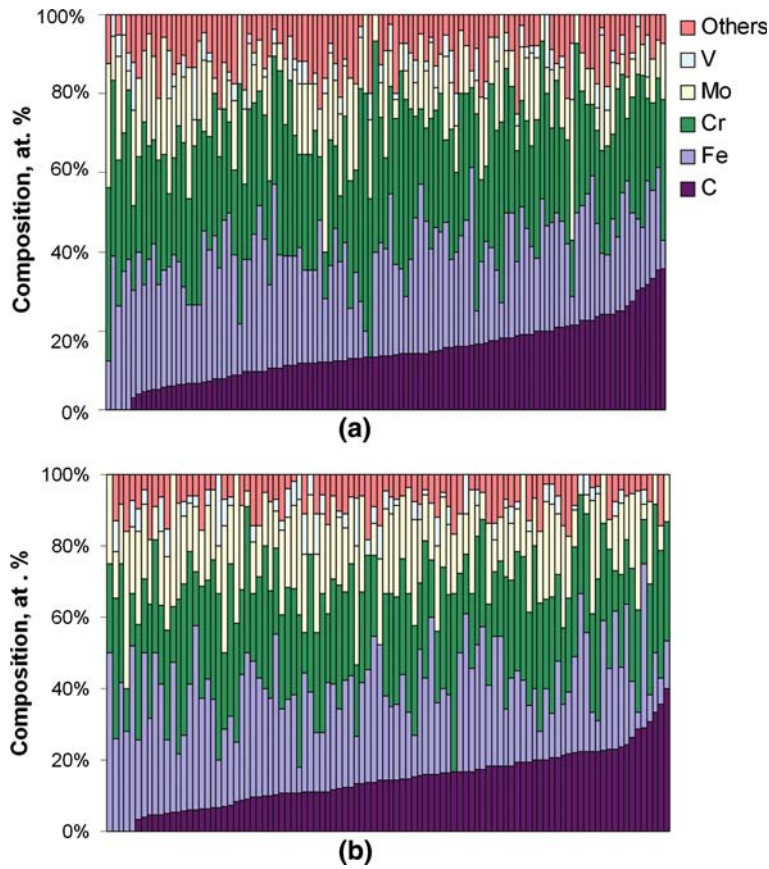


Fig. 10—Stack plots showing the composition of the individual clusters in samples tempered for (a) 4 h and (b) 8 h. There are 111 and 98 particles, respectively, in the two samples.

Table VII. Comparison of the Average Chemical Composition (Atomic Percent) in 4- and 8-Hour Tempered Samples for Carbon-Rich and Carbon-Deficient Clusters; the Error Bar Represents One Standard Deviation

Element	4 h		8 h	
	at. pct C \geq 10	at. pct C $<$ 10	at. pct C \geq 10	at. pct C $<$ 10
Fe	25.06 \pm 8.56	30.45 \pm 7.80	25.38 \pm 10.98	31.04 \pm 11.57
Cr	30.59 \pm 9.85	32.76 \pm 9.28	27.65 \pm 8.28	30.95 \pm 9.55
Mo	13.68 \pm 7.62	18.00 \pm 7.56	18.09 \pm 7.68	21.80 \pm 9.01
V	2.86 \pm 3.33	2.92 \pm 3.94	2.87 \pm 3.26	3.60 \pm 4.58
C	17.68 \pm 6.16	5.67 \pm 3.04	18.28 \pm 6.24	5.78 \pm 3.33

8-hour tempered sample compared to the 4-hour tempered sample.

- Nearly 30 pct of the clusters present in either sample contain less than 10 at. pct carbon and can be considered as intermetallic co-clusters. These might significantly influence both strength and toughness.
- Finer clusters, containing less than 100 detected ions ($r < 0.825$ nm), show a large scatter in their composition, in both the 4- and 8-hour tempered samples. This scatter is likely due to their small size.
- Larger clusters, containing more than 100 detected ions ($r > 0.825$ nm), are all carbon rich (> 10 at. pct C) and exhibit much less scatter in the composition. The largest ones have composition tending

toward $M_2C_{0.8}$. These would be the finest particles that are observed in the TEM.

- From these results, it appears that physical attributes such as size and number density, rather than chemical composition, may be responsible for the enhanced toughness of the 8-hour tempered sample relative to the 4-hour tempered sample.

ACKNOWLEDGMENTS

This research was funded by the Defence Research and Development Organization (DRDO), India, under Project No. DMR-254 "Science and Design of Materials at Atomic Scale." The permission of the Director,

Defence Metallurgical Research Laboratory (DMRL), Hyderabad, to publish the results is gratefully acknowledged. Professor S. Ranganathan, Indian Institute of Science, Bangalore, and Dr. D. Banarjee, Chief Controller, DRDO, are acknowledged for their keen interest, constant encouragement, and guidance throughout the project. Mr. Mohan P. Pathak, DMRL, is also acknowledged for his assistance during 3DAP investigations. The authors also thank the reviewer for many useful comments and suggestions.

REFERENCES

1. M.K. Miller, P. Periege, and M.G. Burke: *Mater. Characterization*, 2000, vol. 44, pp. 235–54.
2. E.V. Pereloma, A. Shekhter, M.K. Miller, and S.P. Ringer: *Acta Mater.*, 2004, vol. 52, pp. 5589–5602.
3. R.C. Thomson: *Mater. Characterization*, 2000, vol. 44, pp. 219–33.
4. K. Seto, D.J. Larson, P.J. Warren, and G.D.W. Smith: *Scripta Mater.*, 1999, vol. 40 (9), pp. 1029–34.
5. M. Hattestrand, J.-O. Nilsson, K. Stiller, P. Liu, and M. Anderson: *Acta Mater.*, 2004, vol. 52, pp. 1023–37.
6. K. Hono: *Progr. Mater. Sci.*, 2002, vol. 47, pp. 621–729.
7. D. Blavette, E. Cadel, and B. Deconihout: *Mater. Characterization*, 2000, vol. 44, pp. 133–57.
8. L.E. Iorio, J.L. Maloney, and W.M. Garrison, Jr.: *40th Mechanical Working and Steel Processing Conf. Proc.*, Vol. XXXVI, ISS-AIME, Warrendale, PA, 1999, pp. 901–20.
9. J.M. Dahl and P.M. Novotny: *Adv. Mater. Processes*, 1999, vol. 155 (3), pp. 23–25.
10. R. Balamuralikrishnan: Ph.D. Thesis, Carnegie Mellon University, Pittsburgh, PA, 1998.
11. W.M. Garrison, Jr. and M.A. Rhoads: *Trans. Ind. Inst. Met.*, 1996, vol. 49 (3), pp. 151–62.
12. M. Srinivas, R. Balamuralikrishnan, R. Veerababu, and K. Muraleedharan: Defence Metallurgical Research Laboratory, Hyderabad, India, unpublished research, 2007.
13. A.J. Allen, D. Gavillet, and J.R. Weertman: *Acta Metall. Mater.*, 1993, vol. 41 (6), pp. 1869–84.
14. G.A. Clarke, W.R. Andrews, J.A. Begley, J.K. Donald, G.T. Embley, J.D. Landes, D.E. McCabe, and J.H. Underwood: *ASTM J. Test. Eval.*, 1979, vol. 7, p. 49.
15. M.K. Miller and G.D.W. Smith: *Atom Probe Microanalysis: Principles and Applications to Materials Problems*, Materials Research Society, Pittsburgh, PA, 1989, pp. 43–50.
16. D. Vaumousse, A. Cerezo, and P.J. Warren: *Ultramicroscopy*, 2003, vol. 95, pp. 215–21.
17. D. Isheim, R. Prakash Kolli, M.E. Fine, and D.N. Seidman: *Scripta Mater.*, 2006, vol. 55, pp. 35–40.
18. E.V. Pereloma, I.B. Timokhina, K.F. Russell, and M.K. Miller: *Scripta Mater.*, 2006, vol. 54, pp. 471–76.
19. M.K. Miller, K.F. Russell, and D.T. Hoelzer: *J. Nucl. Mater.*, 2006, vol. 351 (1–3), pp. 261–68.
20. I.B. Timikhina, P.D. Hodgson, S.P. Ringer, R.K. Zheng, and E.V. Pereloma: *Scripta Mater.*, 2007, vol. 56, pp. 601–04.
21. M.K. Miller, K.F. Russell, M.A. Sokolov, and R.K. Nanstad: *J. Nucl. Mater.*, 2003, vol. 320, pp. 177–83.
22. M.K. Miller, K.F. Russell, M.A. Sokolov, and R.K. Nanstad: *Phil. Mag.*, 2005, vol. 85 (4–7), pp. 401–08.
23. M.K. Miller, R.K. Nanstad, M.A. Sokolov, and K.F. Russell: *J. Nucl. Mater.*, 2006, vol. 351, pp. 216–22.
24. G. Sha and A. Cerezo: *Acta Mater.*, 2004, vol. 52, pp. 4503–16.
25. M.K. Miller, K.F. Russell, M.A. Sokolov, and R.K. Nanstad: *J. Nucl. Mater.*, 2007, vol. 361, pp. 248–61.
26. M.K. Miller, M.A. Sokolov, R.K. Nanstad, and K.F. Russell: *J. Nucl. Mater.*, 2006, vol. 351, pp. 187–96.
27. R. Ayer and P.M. Machmeier: *Metall. Trans. A*, 1993, vol. 24A, pp. 1943–55.
28. M.K. Miller: *Atom Probe Tomography: Analysis at the Atomic Level*, Kluwer Academic/Plenum, New York, NY, 2000.
29. M.K. Miller and K.F. Russell: *J. Nucl. Mater.*, 2007, doi: [10.1016/j.jnucmat.2007.05.003](https://doi.org/10.1016/j.jnucmat.2007.05.003).
30. G.M. Carinci, G.B. Olson, J.A. Liddle, L. Chang, and G.D.W. Smith: *34th Sagamore Army Materials Research Conf. Proc.*, G.B. Olson et al., eds., U.S. Government Printing Office, Washington, DC, 1990, pp. 179–208.
31. J.S. Montgomery and G.B. Olson: *Proc. G.R. Speich Symp.*, G. Krauss and P.E. Repas, eds., ISS, Warrendale, PA, 1992, pp. 177–214.